High-K multiquasiparticle configurations and limiting moments of inertia in ^{178}W

D. M. Cullen, S. L. King, A. T. Reed, and J. A. Sampson
Oliver Lodge Laboratory, Department of Physics, University of Liverpool, Liverpool L69 7ZE, United Kingdom

P. M. Walker, C. Wheldon, and F. Xu
Department of Physics, University of Surrey, Guildford GU2 5XH, United Kingdom

G. D. Dracoulis
Department of Nuclear Physics, RSPhysSE, Australian National University, Canberra, Australian Capital Territory 0200, Australia

I.-Y. Lee, A. O. Macchiavelli, and R. W. MacLeod
Lawrence Berkeley National Laboratory, Berkeley, California 94720

A. N. Wilson* and C. Barton
Wright Nuclear Structure Laboratory, Yale University, 272 Whitney Avenue, New Haven, Connecticut 06511
(Received 2 June 1999; published 26 October 1999)

Three new high-K multiquasiparticle intrinsic states, $K^\pi=(29^+)$, $K^\pi=30^+$, and $K^\pi=(34^+)$, have been assigned in ^{178}W. The configurations of these states are based on ten, eight, and ten, unpaired nucleons, respectively, and they represent the highest-seniority intrinsic K states observed to date. The γ-ray intensity branching ratios and associated $|g_K-g_R|$ values have been used to contribute to the specifications of the underlying single-particle configurations of the states. Configuration-constrained potential energy surface calculations indicate that the nucleus retains stably deformed axially symmetric shapes. This evidence, coupled with the experimental γ-ray decay rates, suggests that K remains a good quantum number in these highest-seniority intrinsic state configurations. The aligned angular momenta of the $K^\pi=(29^+)$, $K^\pi=30^+$, and $K^\pi=(34^+)$ bands are observed to be lower than those of the other eight quasiparticle, $K^\pi=25^+$ and $K^\pi=28^-$ bands in ^{178}W. These differences are interpreted as the effects of reduced pairing due to blocking by the constituent particles. While the dynamic moments of inertia are similar, they remain substantially less than those of a classical rigid rotor, apparently saturating at a value of about $56\hbar^2$ MeV^{-1}.
[S0556-2813(99)03611-0]

PACS number(s): 27.70.+q, 21.10.Jx, 21.10.Re

I. INTRODUCTION

It has long been established that the reduced moments of inertia observed for rotational bands in deformed nuclei are a consequence of the nuclear pairing force [1–4]. This force is responsible for coupling pairs of nucleons together in an analogous manner to the paired electrons in the BCS theory of superconductors [5]. However, the analogy is restricted because nuclei are finite systems and the pairing correlations involve only a few particles. Recently, much evidence has been presented for the demise of nuclear pairing correlations on the basis of increasing angular momentum [6]. In this case the Coriolis force destroys the pairing correlations gradually (unlike the first-order phase transitions observed in superconductors). In contrast, the demise of pairing correlations based on the number of unpaired nucleons (the seniority of the state) is not so well established. As the nuclear pairing force becomes quenched with increasing seniority, the nuclear moment of inertia is observed [7] to increase toward that of a classical rigid body, although shell effects may be important [8]. The large number of high-K multiquasiparticle states identified in ^{178}W [9,10] have offered a unique opportunity to study this effect and an extension of the available experimental information would be valuable.

The highest-K rotational band, prior to this experiment, was the $K^\pi=28^-$ eight-quasiparticle band in ^{178}W [9]. There are, however, predictions [11] that higher-K states should compete to form the yrast line in ^{178}W. This paper discusses the search for higher-seniority states in ^{178}W, the observation of an eight-quasiparticle $K^\pi=30^+$ band, and candidates for the ten-quasiparticle $K^\pi=29^+$ and $K^\pi=34^+$ states. It is significant that the $K^\pi=30^+$ and $K^\pi=(34^+)$ configurations do not include the alignable $h_{9/2}$ proton (which has been noted to mask alignment and moment-of-inertia changes when it is a component of a multiquasiparticle configuration [7]), giving improved insight into the influence of seniority on moments of inertia.

II. EXPERIMENT

High-spin states were populated in ^{178}W with the ^{170}Er(^{13}C,5n) reaction. The ^{13}C beam was supplied by the 88-inch cyclotron at the Lawrence Berkeley National Laboratory and the data were recorded with the one hundred and two escape-suppressed germanium detectors of the GAMMASPHERE array [12]. The natural beam pulsing frequency of 5.66 MHz resulted in a beam pulse every 177 ns. Energy and efficiency calibrations were obtained with ^{133}Ba and ^{152}Eu sources which were placed at the target position. Ta and Cu absorbers of thickness $\approx$0.1 mm were used in front of the

*Present address: Department of Physics, University of York, Heslington, York YO10 5DD, U.K.

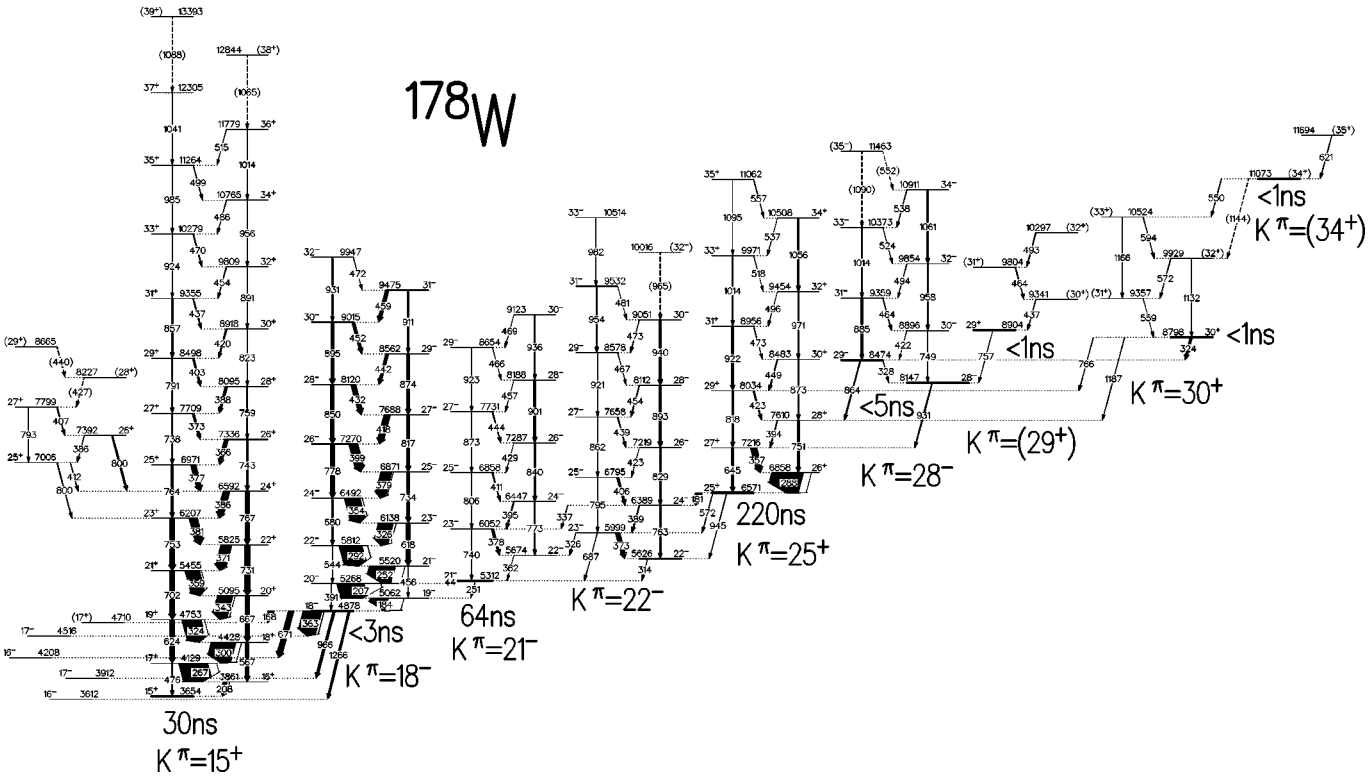

FIG. 1. Partial level scheme for ^{178}W showing the extension to the high-K states for $K \geqslant 15$. All of the lower-seniority bands have also been extended. It should also be noted that the maximum input angular momentum of the reaction was about $40\hbar$.

germanium detectors to reduce the number of x rays being detected.

The experiment was performed in two complementary parts. First, a thick target of ^{170}Er (enriched to 96.88%) with thickness 4.6 mg/cm^2 was used. This stopped most of the nuclear recoils in the focus of the array. A 0.25-pnA beam with energy 86 MeV was used and a total of 9.7×10^{10} unpacked triple-coincident events were collected. The second part of the experiment utilized a thin target of ^{170}Er (enriched to 96.88%) with a thickness of 0.6 mg/cm^2, in order to enhance the observation of the higher-spin states in ^{178}W. A 5-pnA beam with energy 83 MeV was used with this target and a total of 3.6×10^{10} unpacked triple-coincident events were collected. The beam current was adjusted in both cases to limit the singles rate in the individual germanium detectors to 4–5 kHz, which resulted in an event rate of approximately 15 kHz. The γ-γ coincidence timing window was defined such that the maximum time difference between any two germanium detectors was 1 μs.

III. DATA ANALYSIS AND RESULTS

The partial level scheme for states above the $K=15$ isomer at 3654 keV in ^{178}W is shown in Fig. 1. The states with $K \leqslant 15$ were also extended to higher spin. For example, two new transitions (1013 and 1037 keV) are assigned as the $32^+ \rightarrow 30^+$ and $34^+ \rightarrow 32^+$ members of the ground-state band, respectively. The scheme was deduced from a variety of two-, three-, and four-dimensional histograms. The use of one hundred and two escape-suppressed spectrometers yielded triple or higher-fold γ-ray events. The time coincidence information, with respect to the beam pulsing of the cyclotron, enabled various delayed-early (across isomer) histograms to be created. In particular, a delayed-early matrix was constructed from gating on the delayed 763-, 389-, and 373-keV transitions, which lie below the 220 ns $K^\pi=25^+$ isomer, and selecting any prompt transitions (± 29 ns from the primary beam pulse), which were part of the same event. Gates were placed in these histograms and the γ-ray intensities and coincidence relationships were used to determine the order of the γ rays in the level scheme. These data were analyzed using both the ''RADWARE'' [13] and the ''UPAK'' [14] software packages. Tables I and II list the energies and intensities for the transitions in the $K^\pi=15^+$ band and those above the $K^\pi=25^+$ state at 6571 keV, respectively. Figures 2(a)–2(d) show selected spectra for the $K^\pi=15^+$, $K^\pi=25^+$, $K^\pi=28^-$, and $K^\pi=30^+$ bands in these data, respectively. In the analysis it was noted that the thin-target reaction data were useful in extending the level scheme to higher rotational frequencies using the four-dimensional histogram.

The multipolarities of the γ rays were obtained from an angular correlation analysis using the method of directional correlation from oriented states (DCO) [15]. The directional correlation ratios extracted from these matrices,

$$R_{DCO}=\frac{I_\gamma(\text{forward})+I_\gamma(\text{backward})}{I_\gamma(90^\circ)}, \qquad (1)$$

were used to deduce the multipolarity of the γ rays, except for the weaker transitions. The DCO ratios (see Tables I and

TABLE I. γ-ray energies, intensities, DCO ratios, and spin assignments for the transitions in the $K^{\pi}=15^{+}$ band in ^{178}W. The intensities are normalized to the intensity of the 267-keV transition whose intensity is about 4% of the ground-state band $4^{+}\rightarrow 2^{+}$ transition. It should be noted that the DCO ratios for the $\Delta I=1$ transitions correspond to generally mixed ($M1/E2$) multipolarities.

Band, K^{π}	$E_{\gamma}\pm\Delta E_{\gamma}$	$I_{\gamma}\pm\Delta I_{\gamma}$	R_{DCO}	$I_i^{\pi}\rightarrow I_f^{\pi}$
15^{+}	207.5±0.1	141±13	0.87±0.02	$16^{+}\rightarrow 15^{+}$
15^{+}	267.4±0.1	1000±31	0.58±0.03	$17^{+}\rightarrow 16^{+}$
15^{+}	299.7±0.1	854±27	1.10±0.04	$18^{+}\rightarrow 17^{+}$
15^{+}	323.8±0.1	659±21	1.15±0.04	$19^{+}\rightarrow 18^{+}$
15^{+}	343.1±0.1	525±16	1.11±0.04	$20^{+}\rightarrow 19^{+}$
15^{+}	358.8±0.1	498±16	1.16±0.05	$21^{+}\rightarrow 20^{+}$
15^{+}	365.5±0.1	116±5	1.15±0.06	$26^{+}\rightarrow 25^{+}$
15^{+}	371.1±0.1	339±12	1.28±0.06	$22^{+}\rightarrow 21^{+}$
15^{+}	373.0±0.1	60±6	1.15±0.08	$27^{+}\rightarrow 26^{+}$
15^{+}	377.4±0.1	160±7		$25^{+}\rightarrow 24^{+}$
15^{+}	380.8±0.1	257±9		$23^{+}\rightarrow 22^{+}$
15^{+}	385.8±0.1	203±16		$24^{+}\rightarrow 23^{+}$
15^{+}	387.5±0.1	78±8		$28^{+}\rightarrow 27^{+}$
15^{+}	403.2±0.1	45±4		$29^{+}\rightarrow 28^{+}$
15^{+}	419.6±0.6			$30^{+}\rightarrow 29^{+}$
15^{+}	420.3±0.3	41±4		$26^{+}\rightarrow 25^{+}$
15^{+}	436.9±0.2	26±4		$31^{+}\rightarrow 30^{+}$
15^{+}	453.9±0.3	22±4		$32^{+}\rightarrow 31^{+}$
15^{+}	469.5±0.3	23±4		$33^{+}\rightarrow 32^{+}$
15^{+}	475.6±0.4	30±6		$17^{+}\rightarrow 15^{+}$
15^{+}	566.8±0.2	106±8	0.92±0.12	$18^{+}\rightarrow 16^{+}$
15^{+}	623.6±0.1	149±8	1.26±0.10	$19^{+}\rightarrow 17^{+}$
15^{+}	667.1±0.1	145±8	1.10±0.11	$20^{+}\rightarrow 18^{+}$
15^{+}	702.4±0.1	168±8	1.18±0.07	$21^{+}\rightarrow 19^{+}$
15^{+}	730.5±0.1	183±9	1.14±0.07	$22^{+}\rightarrow 20^{+}$
15^{+}	737.5±0.2	42±5		$27^{+}\rightarrow 25^{+}$
15^{+}	743.0±0.2	59±6	0.83±0.13	$26^{+}\rightarrow 24^{+}$
15^{+}	752.5±0.1	170±8	1.16±0.08	$23^{+}\rightarrow 21^{+}$
15^{+}	758.9±0.1	22±5		$28^{+}\rightarrow 26^{+}$
15^{+}	764.3±0.2	81±8	1.13±0.13	$25^{+}\rightarrow 23^{+}$
15^{+}	767.3±0.1	135±9	1.18±0.10	$24^{+}\rightarrow 22^{+}$
15^{+}	791.1±0.4	38±6		$27^{+}\rightarrow 25^{+}$
15^{+}	823.4±0.4			$30^{+}\rightarrow 28^{+}$
15^{+}	836.0±0.4	33±6		$28^{+}\rightarrow 26^{+}$
15^{+}	856.7±0.2	51±4		$31^{+}\rightarrow 29^{+}$
15^{+}	891.2±0.2	63±5		$32^{+}\rightarrow 30^{+}$
15^{+}	924.0±0.3	38±4		$33^{+}\rightarrow 31^{+}$
15^{+}	386.0±1.0	10±13		$26^{+}\rightarrow 25^{+}$
15^{+}	406.6±0.2	21±4		$27^{+}\rightarrow 26^{+}$
15^{+}	411.7±0.4	19±5		$25^{+}\rightarrow 24^{+}$
15^{+}	427.0±0.2	15±4		$28^{+}\rightarrow 27^{+}$
15^{+}	439.5±0.4	19±4		$29^{+}\rightarrow 28^{+}$
15^{+}	793.1±1.4			$29^{+}\rightarrow 27^{+}$
15^{+}	799.7±0.7	31±16		$25^{+}\rightarrow 23^{+}$
15^{+}	799.9±0.6	35±16		$26^{+}\rightarrow 24^{+}$

II) were compared with a selection of known stretched quadrupole transitions and known pure ($\delta=0$) dipole transitions whose ratios were ≈ 1.0 and ≈ 0.6, respectively. Some of the high-spin band extensions are assumed to be electric quadrupole transitions on the basis of the regularly spaced γ-ray energy sequences, which are characteristic of quadrupole rotation.

The analysis and discussion of these data will concentrate

TABLE II. γ-ray energies, intensities, DCO ratios, and spin assignments for the transitions in the $K^\pi = 25^+$, $K^\pi = 28^-$, $K^\pi = (29^+)$, $K^\pi = 30^+$, and $K^\pi = (34^+)$ bands in ^{178}W. The intensities were extracted from a series of fits in the early-delayed gated matrix and are normalized to the intensity of the 358-keV transition. It should be noted that these DCO ratios are sometimes mixed, for example, the 287.8-keV $M1/E2$ transition has a DCO ratio of 0.17 ± 0.01. The absolute intensity of the 931.2-keV transition is approximately 1% of the $4^+ \rightarrow 2^+$, 351-keV transition in the ground-state band.

Band, K^π	$E_\gamma \pm \Delta E_\gamma$	$I_\gamma \pm \Delta I_\gamma$	R_{DCO}	$I_i^\pi \rightarrow I_f^\pi$
25^+	287.8±0.1	1347±42	0.17±0.01	$26^+ \rightarrow 25^+$ $M1$
25^+	357.2±0.1	1000±11	1.05±0.03	$27^+ \rightarrow 26^+$ $M1$
25^+	394.3±0.1	589±29	1.52±0.06	$28^+ \rightarrow 27^+$ $M1$
25^+	423.6±0.1	251±56	2.16±0.16	$29^+ \rightarrow 28^+$ $M1$
25^+	449.3±0.1	282±58		$30^+ \rightarrow 29^+$ $M1$
25^+	473.4±0.1	116±27		$31^+ \rightarrow 30^+$ $M1$
25^+	496.1±0.1	106±10	1.12±0.05	$32^+ \rightarrow 31^+$ $M1$
25^+	517.7±0.3	71±16		$33^+ \rightarrow 32^+$ $M1$
25^+	536.9±0.3	29±11		$34^+ \rightarrow 33^+$ $M1$
25^+	556.5±0.3	—		$35^+ \rightarrow 34^+$ $M1$
25^+	645.0±0.1	261±17	1.21±0.05	$27^+ \rightarrow 25^+$ $E2$
25^+	751.2±0.2	375±6	1.53±0.17	$28^+ \rightarrow 26^+$ $E2$
25^+	817.9±0.1	254±5	1.03±0.14	$29^+ \rightarrow 27^+$ $E2$
25^+	873.2±0.2	221±6	1.10±0.09	$30^+ \rightarrow 28^+$ $E2$
25^+	923.4±0.2	182±5		$31^+ \rightarrow 29^+$ $E2$
25^+	970.7±0.2	205±6	0.78±0.03	$32^+ \rightarrow 30^+$ $E2$
25^+	1014.1±0.1	84±10		$33^+ \rightarrow 31^+$ $E2$
25^+	1055.5±0.3	91±10		$34^+ \rightarrow 32^+$ $E2$
25^+	1095.5±0.7	30±10	1.28±0.36	$34^+ \rightarrow 32^+$ $E2$
28^+	327.7±0.1	198±13	0.20±0.05	$29^- \rightarrow 28^-$ $M1$
28^+	421.5±0.1	95±3		$30^- \rightarrow 29^-$ $M1$
28^+	463.6±0.2	79±21		$31^- \rightarrow 30^-$ $M1$
28^+	493.7±0.8	—		$32^- \rightarrow 31^-$ $M1$
28^+	524.0±0.2	—		$33^- \rightarrow 32^-$ $M1$
28^+	537.6±0.1	—		$34^- \rightarrow 33^-$ $M1$
28^+	748.9±0.1	—		$30^- \rightarrow 28^-$ $E2$
28^+	884.8±0.2	45±9		$31^- \rightarrow 29^-$ $E2$
28^+	957.6±0.2	—		$32^- \rightarrow 30^-$ $E2$
28^+	1017.7±0.7	—		$33^- \rightarrow 31^-$ $E2$
28^+	1060.5±0.7	—		$34^- \rightarrow 32^-$ $E2$
28^+	324.4±0.1	181±12	0.60±0.11	$30^+ \rightarrow 29^-$ $E1$
28^+	864.4±0.1	153±9	0.68±0.13	$29^- \rightarrow 28^+$ $E1$
28^+	931.2±0.1	274±20	0.62±0.03	$28^- \rightarrow 27^+$ $E1$
(29^+)	757.2±0.2	74±7	0.75±0.24	$(29^+) \rightarrow 28^-$ $E1$
(29^+)	437.0±0.1	64±6		$(30^+) \rightarrow (29^+)$ $M1$
(29^+)	464.0±0.1	25±4		$(31^+) \rightarrow (30^+)$ $M1$
(29^+)	492.9±0.1	29±4		$(32^+) \rightarrow (31^+)$ $M1$
(29^+)	483.9±0.2	19±4		$(33^+) \rightarrow (31^+)$ $M1$
30^+	559.1±0.1	100±8	1.07±0.17	$31^+ \rightarrow 30^+$ $M1$
30^+	572.4±0.1	58±7	0.48±0.10	$32^+ \rightarrow 31^+$ $M1$
30^+	594.1±0.2	33±5	1.11±0.05	$33^+ \rightarrow 32^+$ $M1$
30^+	765.8±0.1	46±6	1.10±0.20	$30^+ \rightarrow 29^+$ $M1$
30^+	1132.0±0.5	5±1		$(32^+) \rightarrow (30^+)$ $E2$
30^+	1166.1±0.4	10±2		$(33^+) \rightarrow (31^+)$ $E2$
30^+	1187.3±0.4	11±1		$30^+ \rightarrow 28^+$ $E2$
(34^+)	549.6±0.1	35±5		$(34^+) \rightarrow (33^+)$ $M1$
(34^+)	621.7±0.1	32±6		$(35^+) \rightarrow (34^+)$ $M1$

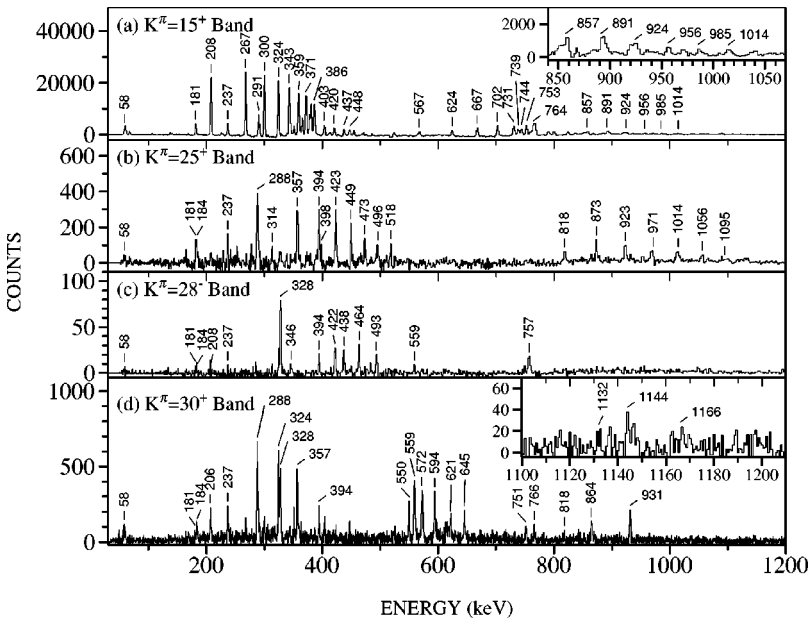

FIG. 2. Spectra for (a) a sum of all combinations of triple gates in the $K^{\pi}=15^{+}$ band, (b) a sum of all combinations of triple gates in the $K^{\pi}=25^{+}$ band, (c) a triple gated spectrum (288-, 356-, and 931-keV transitions) for the $K^{\pi}=28^{-}$ band, and (d) a sum of single gates (324-, 549-, 559-, 572-, 595-, and 621-keV transitions) in the $K^{\pi}=30^{+}$ band from the early delayed matrix.

on the highest-seniority states with $K \geqslant 15$. The lower-seniority states have been well studied recently in Ref. [10]. In the present work all of the multiquasiparticle rotational bands with $K \geqslant 15$ have been extended to higher rotational frequencies (see Fig. 1). For example, the band built upon the $K^{\pi}=15^{+}$ state has been extended from spin 25 to spin 39. A γ-ray spectrum of this band is shown in Fig. 2(a). This extension of the band encompasses a band crossing and represents the highest-K, highest-seniority band crossing, where the entire alignment gain has been observed. In addition, candidates for the first few states in the continuation of the lower-seniority band to rotational frequencies above the crossing are also observed, as shown on the left-hand side of Fig. 1.

The $K^{\pi}=18^{-}$, $K^{\pi}=21^{-}$, and $K^{\pi}=22^{-}$ bands have all been extended in this work to higher rotational frequencies. Some new transitions have also been observed which link these bands to the lower-spin states and thereby remove ambiguities in the previous configuration assignments [10]. For example, in the $K^{\pi}=18^{-}$ band, the new observation of the two lowest $E2$ transitions in the band (391 and 456 keV) allow the bandhead spin and parity to be firmly placed as 18^{-}. Similarly, the observation of the 740 keV $23^{-} \rightarrow 21^{-}$ transition in the $K^{\pi}=21^{-}$ band is consistent with the 21^{-} bandhead spin and parity assignment.

The states in the $K^{\pi}=25^{+}$ band have been extended over those established in Refs. [9,10] [see Figs. 1 and 2(b)]. A new transition of 864 keV was observed to feed into this band at the 28^{+} state, linking it to the 29^{-} state in the $K^{\pi}=28^{-}$ band as discussed below. The states in the $K^{\pi}=28^{-}$ band have been extended and reordered over those discussed in Refs. [9,10] above spin 30. A spectrum of this band is shown in Fig. 2(c). The assignment of $K^{\pi}=28^{-}$ is confirmed by the multipolarity of the linking transitions from the DCO results given in Table II. The 931-keV transition has a DCO ratio of 0.62 ± 0.03, which is consistent with it being a pure dipole transition, and since it shows little mixing, it is likely to be an $E1$ transition. Similarly, the 864-keV linking transition, discussed above, has a DCO ratio of 0.68 ± 0.13 and is also assumed to be an $E1$ transition. A new intrinsic state was also observed at an excitation energy of 8904 keV. This state decays by a 757-keV transition to the $K^{\pi}=28^{-}$ bandhead state at 8147 keV. The large uncertainty, 32%, in the DCO ratio for this transition does not permit a definite multipolarity to be established, hence a tentative assignment of $K^{\pi}=(29^{+})$ is given in Fig. 1. The associated in-band $E2$ transitions were not observed and were reasoned to be below the sensitivity of the present experiment.

In the analysis a new intrinsic state at an excitation energy of 8798 keV was observed. This state, assigned as $K^{\pi}=30^{+}$, is connected by a 324-keV transition to the 29^{-} state in the known $K^{\pi}=28^{-}$ band, and by 766-keV and 1187-keV transitions to the 29^{+} and 28^{+} states in the $K^{\pi}=25^{+}$ band, respectively. The assignment of $K^{\pi}=30^{+}$ arises from the use of the DCO ratio of the 324-keV γ-ray linking transition, 0.60 ± 0.11, to deduce its $E1$ nature. The 766-keV γ-ray linking transition has a DCO ratio of 1.10 ± 0.20, which is consistent with a mixed $I \rightarrow I-1$, $M1/E2$ assignment, albeit with a large uncertainty. The spin and parity of this $K^{\pi}=30^{+}$ state are, however, firmly established due to the combination of the observed $E1$, $M1$, and $E2$ transitions. Any other assignment is much more unlikely based on transition rate arguments. For example, if the 1187-keV transition were $M2$ (which would be K-forbidden), then a measurable half-life would be expected. Figure 2(d) shows a spectrum of the $K^{\pi}=30^{+}$ band and from the inset it can be observed that the in-band $E2$ transitions are very weak. In addition, in coincidence with the highest-spin transitions in the band, a 550-keV transition is observed to connect this band to a new state at an excitation energy of 11 073 keV [see Fig. 2(d)]. This new state is a candidate for a $K^{\pi}=(34^{+})$ intrinsic state which would represent the highest-K, highest-seniority intrinsic state observed to date and is the first intrinsic state above 10-MeV excitation energy to be observed in a well-deformed nucleus. The 621-keV transition is tentatively as-

TABLE III. $|g_K-g_R|$ ratios for the transitions in the $K^\pi=15^+$, $K^\pi=25^+$, $K^\pi=28^-$, and $K^\pi=30^+$ bands in ^{178}W. These calculations assume Q_o is 7.0 *e* b and the data are from a combination of the four-dimensional and the early delayed analysis.

Spin ($\hbar$)	$\lvert g_K-g_R\rvert$
$K^\pi=15^+$ band	
17.0	0.069±0.015
18.0	0.060±0.005
19.0	0.059±0.004
20.0	0.065±0.004
21.0	0.067±0.004
22.0	0.059±0.003
23.0	0.058±0.003
24.0	0.063±0.005
25.0	0.076±0.008
26.0	0.076±0.009
27.0	0.063±0.009
28.0	0.119±0.043
29.0	0.067±0.011
31.0	0.045±0.008
$K^\pi=25^+$ band	
27.0	0.094±0.011
28.0	0.084±0.009
29.0	0.103±0.010
30.0	0.148±0.012
31.0	0.084±0.025
32.0	0.047±0.126
$K^\pi=28^-$ band	
31.0	0.057±0.023
32.0	0.067±0.046
33.0	0.088±0.061
34.0	0.098±0.049
$K^\pi=30^+$ band	
32.0	0.257±0.037
33.0	0.188±0.028

sumed to be the first member of the rotational band that is expected be built upon this state.

IV. DISCUSSION

A. $|g_K-g_R|$ ratios

In order to evaluate the configurations of the bands, it is useful to compare the experimentally determined $|g_K-g_R|$ values with the theoretical predictions from the geometric model of Dönau and Frauendorf [16]. The experimental $|(g_K-g_R)/Q_\bigcirc|$ values have been deduced from the $\Delta I=2$ to $\Delta I=1$ γ-ray intensity branching ratios (see Table III). The amount of quadrupole admixture in the dipole ($\Delta I=1$) transitions was calculated in the strong-coupling limit of the rotational model with

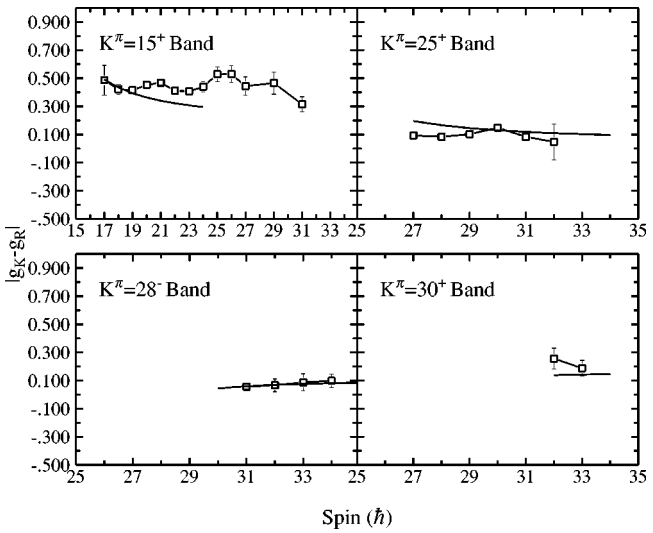

FIG. 3. $|g_K-g_R|$ values for the $K^\pi=15^+$, $K^\pi=25^+$, $K^\pi=28^-$, and $K^\pi=30^+$ bands in ^{178}W. Also shown are theoretically calculated values by the solid lines. In the experimental values, a quadrupole moment of $Q_o=7$ *e* b was assumed and, in addition, the sign of g_K-g_R is ambiguous. The data are from a combination of the four-dimensional and the delayed-early analysis. Where no error bars are shown, the uncertainties are smaller than the size of the data points.

$$\frac{\delta^2}{(1+\delta^2)}=\frac{2K^2(2I-1)}{(I+1)(I-1+K)(I-1-K)}\frac{E_1^5}{E_2^5}\frac{I_2^\gamma}{I_1^\gamma}, \qquad (2)$$

where δ is the quadrupole/dipole mixing ratio, E and I^γ respectively refer to the transition energies (in MeV) and intensities, and the subscripts 1,2 refer to $\Delta I=1,2$ transitions, respectively. The ratio of the g factors to the quadrupole moment $Q_\bigcirc$ is calculated by

$$\frac{g_K-g_R}{Q_\bigcirc}=0.933\frac{E_1}{\delta\sqrt{I^2-1}}. \qquad (3)$$

Equation (2) assumes a well-defined K value and only yields the magnitude of δ and not its sign. In this work, the sign of $|g_K-g_R|$ remains ambiguous because it was not possible to measure angular correlation ratios to determine δ for the low-intensity transitions in the band. However, the positive sign of δ was deduced from a comparison with the angular distribution measurements for the transitions in Ref. [10] and the theoretical estimates. The ratios for the $K^\pi=15^+$, $K^\pi=25^+$, $K^\pi=28^-$ and $K^\pi=30^+$ bands, assuming $Q_0=7e$b, are shown in Figs. 3(a)–3(d). For some of the states in these bands, it was not always possible to extract accurate ratios because the intensities of the transitions were too weak.

In the theoretical calculations, based on the geometric model of Dönau and Frauendorf [16], the ratio of reduced transition probabilities for the $\Delta I=1$ to $\Delta I=2$ transitions was calculated from

TABLE IV. Parameters used in the theoretical $B(M1)/B(E2)$ ratio calculation from the geometric model (see text for details). Additionally, the quadrupole moment was taken to be 7.0 e b, $\gamma = 0°$, and $g_R = Z/A$.

Neutron state	Shell	g factor	Alignment, i_x	K
$[512]5/2^-$	$f_{7/2}$	-0.328	0.0	2.5
$[633]7/2^+$	$i_{13/2}$	-0.177	5.4	3.5
$[514]7/2^-$	$h_{9/2}$	0.209	0.0	3.5
$[624]9/2^+$	$i_{13/2}$	-0.177	0.0	4.5
$[521]1/2^-$	$f_{5/2}$	0.328	0.0	0.5
$[503]7/2^-$	$f_{7/2}$	-0.328	0.0	3.5
$[541]1/2^-$	$h_{9/2}$	0.786	2.5	0.5
$[402]5/2^+$	$d_{5/2}$	1.470	0.0	2.5
$[404]7/2^+$	$g_{7/2}$	0.739	0.0	3.5
$[514]9/2^-$	$h_{11/2}$	1.214	0.0	4.5
$[505]11/2^-$	$h_{11/2}$	1.214	0.0	5.5

$$\frac{B(M1:I\rightarrow I-1)}{B(E2:I\rightarrow I-2)} = \frac{12}{5Q_0^2\cos^2(\gamma+30°)}\left[1-\frac{K^2}{1-\left(\frac{1}{2}\right)^2}\right]^{-2} \times\left\{\left(1-\frac{K^2}{I^2}\right)^{1/2}\left[K_1(g_1-g_R) \times\left(1\pm\frac{\Delta e'}{\hbar\omega}\right)+\sum_n K_n(g_n-g_R)\right] - \frac{K}{I}\left[(g_1-g_R)i_n+\sum_n (g_n-g_R)i_n\right]\right\}^2, \tag{4}$$

where

$$K = K_1 + K_2 + K_3 + \cdots. \tag{5}$$

The subscripts n refer to the quasiparticles that couple to form the band and $\Delta e'$ is the signature splitting in the level energies in the rotating frame. The values used for the g factors, alignments, i_x and K values for each band, are tabulated in Table IV. These $B(M1:I\rightarrow I-1)/B(E2:I\rightarrow I-2)$ values were converted to $|g_K - g_R|$ with

$$|g_K - g_R| = \pm\frac{Q_0}{K}\sqrt{\frac{5}{12}\frac{B(M1:I\rightarrow I-1)}{B(E2:I\rightarrow I-2)}\frac{\langle IK20|I-2K\rangle^2}{\langle IK10|I-1K\rangle^2}} \tag{6}$$

and are shown as solid lines in Fig. 3. Good agreement with the proposed single-particle configurations is observed for all of the bands. Note that the $|g_K - g_R|$ values for the $K^\pi = 15^+$ band are calculated below the band crossing and are only shown up to a spin where the configuration is valid.

B. Quasiparticle calculations of energies and shapes

In order to estimate the validity of the proposed underlying quasiparticle configurations of the high-K intrinsic states in ^{178}W, the experimental excitation energies have been compared with those predicted from theoretical calculations. The theoretical values were calculated from potential energy surfaces with the method of Xu *et al.* [17] for the specific configurations that are expected to be low in energy from the fixed-deformation calculations [11]. The shape calculations use the Woods-Saxon potential and Lipkin-Nogami pairing. For each quasiparticle configuration the occupied orbitals are fixed (diabatic blocking) and the quadrupole and hexadecapole deformations, β_2, β_4, and γ, are varied in order to minimize the excitation energy. The monopole pairing strength is determined self-consistently, by fitting the odd-even mass differences, while allowing the different ground states to have different shapes. Residual nucleon-nucleon interactions are not taken into account, but these do not affect the calculated shapes.

The specific quasiparticle configurations are given in Table V, where the experimental and calculated bandhead energies are compared. There has been no attempt to obtain detailed energy fits. (The calculations contain no adjustable parameters and no residual interactions.) Rather, the emphasis has been on obtaining realistic, configuration-constrained shape parameters. Table VI shows the results of the calculation in more detail, giving shape parameters, pairing ener-

TABLE V. Predictions for the excitation energies and configurations of ^{178}W intrinsic states. The experimentally observed excitation energies are also shown for comparison. The neutron states are $1/2^-[521]$, $5/2^-[512]$, $7/2^-[514]$, $\mathbf{7/2^+}[633]$, $\mathbf{9/2^+}[624]$, and $7/2^{-(a)}[503]$. The proton states are $\mathbf{1/2^-}[541]$, $5/2^+[402]$, $7/2^+[404]$, $9/2^-[514]$, and $11/2^-[505]$. The bold type indicates an aligning quasiparticle ($h_{9/2}$ proton or $i_{13/2}$ neutron).

K^π	Configuration		E (keV)	
	Neutron	Proton	Expt.	Calc.
15^+	$\mathbf{7/2^+}$,$7/2^-$,	$7/2^+$,$9/2^-$	3653	3720
25^+	$5/2^-$,$\mathbf{7/2^+}$,$7/2^-$,$\mathbf{9/2^+}$	$\mathbf{1/2^-}$,$5/2^+$,$7/2^+$,$9/2^-$	6571	6660
28^-	$1/2^-$,$\mathbf{7/2^+}$,$7/2^-$,$\mathbf{9/2^+}$	$\mathbf{1/2^-}$,$7/2^+$,$9/2^-$,$11/2^-$	8147	8520
29^+	$5/2^-$,$\mathbf{7/2^+}$,$7/2^-$,$\mathbf{9/2^+}$,$1/2^-$,$7/2^{-(a)}$	$\mathbf{1/2^-}$,$5/2^+$,$7/2^+$,$9/2^-$	8904	9490
30^+	$5/2^-$,$\mathbf{7/2^+}$,$7/2^-$,$\mathbf{9/2^+}$	$5/2^+$,$7/2^+$,$9/2^-$,$11/2^-$	8798	8090
34^+	$5/2^-$,$\mathbf{7/2^+}$,$7/2^-$,$\mathbf{9/2^+}$,$1/2^-$,$7/2^{-(a)}$	$5/2^+$,$7/2^+$,$9/2^-$,$11/2^-$	11 073	10 460

TABLE VI. Calculated properties of the bandhead states in ^{178}W (see text for details). In all cases, $\gamma < 2^0$.

K^π	β_2	β_4	Δ_n (keV)	Δ_p (keV)	Q_0 (e b)
0^+	0.241	−0.035	1017	1251	7.1
15^+	0.249	−0.032	769	947	7.5
25^+	0.261	−0.027	579	693	8.0
28^-	0.256	−0.023	579	713	7.7
29^+	0.244	−0.011	480	707	7.6
30^+	0.232	−0.031	599	707	6.6
34^+	0.215	−0.017	487	715	6.2

gies, and the quadrupole moments derived from the shapes. In each case, the values are given for the lowest-energy state of spin and parity that best corresponds to the experimental state.

Although the excitation energy comparisons are generally good (the lower-K states have been compared by Xu *et al.* [17]) it is notable that the $K^\pi = 30^+$ state is observed 708 keV higher than calculated. With the fixed-shape, Nilsson-plus-BCS calculations of Jain *et al.* [11] (including residual interactions), the difference is even greater, 860 keV. There appears to be a limited predictive power for the calculation of excitation energies at very high seniority, and further work is needed to understand the origin of the discrepancy.

The calculated shapes are also of interest. These are sensitive to the configurations, but not to the excitation energies as such. The $K^\pi = 25^+$ state [17] has one of the largest β_2 deformations (0.261) in ^{178}W, while the $K^\pi = 34^+$ state is predicted to have the smallest β_2 value (0.215). The principal difference lies in the change in orbital occupation, from the prolate-driving $1/2^-[541]$ proton orbital, to the oblate driving $11/2^-[505]$ proton orbital. Nevertheless, the shape difference effect on the rigid-body moments of inertia would be small (less than 2%) and, for each configuration, axial symmetry is preserved ($\gamma \approx 0^0$) indicating that the K quantum number should remain valid. The angular-momentum limit to the K quantum number does not yet appear to have been reached. However, in the absence of sufficiently K-forbidden transitions to generate significant half-lives above the $K^\pi = 25^+$ isomer (see the following section), it is not yet possible to test this aspect of the ^{178}W shape calculations for $K > 25$.

C. Half lives and transition rates

The lifetimes of the intrinsic states in ^{178}W are expected to be strongly influenced by the K-selection rule. Any transition which has $\Delta K > \lambda$, the transition multipolarity, is forbidden or retarded, however, the lifetimes of the $K^\pi = 28^-$, $K^\pi = (29^+)$, $K^\pi = 30^+$, and $K^\pi = (34^+)$ intrinsic states are all determined to be short, $\leqslant$ a few ns. This limit results from the fact that gates placed on transitions above the bandhead state are observed in prompt coincidence with those below the bandhead state in the thin target reaction data. If the lifetime of the intrinsic state was longer than a few ns then the nuclear recoils would decay after they had recoiled out of the focus of the germanium detectors and, therefore, would not have been detected. A centroid-shift analysis, similar to that performed in Ref. [10], of the time difference between two germanium events, one gated above and the other gated below the state of interest, was also performed. However, the large volumes of the GAMMASPHERE detectors are not suited for measuring such short half lives (< 1 ns) and consequently only upper limit half lives of < 1 ns could be determined for the $K^\pi = 28^-$, $K^\pi = (29^+)$, $K^\pi = 30^+$, and $K^\pi = (34^+)$ intrinsic states, respectively.

TABLE VII. Hindrance calculation for the γ-ray decays from the $K^\pi = 28^-$, (29^+), 30^+, and (34^+) intrinsic states in ^{178}W. Note that only half-life limits are known, which result in hindrance factor limits (see text for details).

K^π	E_γ (keV)	$T^\gamma_{1/2}$ (ns)	ΔK	$M\lambda$	F_W	f_ν
28^-	931.2	< 1.0	3	$E1$	$< 3.8 \times 10^6$	< 20 [a]
(29^+)	757.2	< 1.2	1	$E1$	$< 2.5 \times 10^6$	
30^+	1189.0	< 22	5	$E2$	< 5529	< 18
30^+	765.8	< 5.2	3	$M1$	$< 106\,967$	< 18
30^+	324.4	< 1.3	2	$E1$	$< 211\,721$	< 21 [a]
(34^+)	549.6	< 0.6	4	$M1$	< 4585	< 17

[a]The general hindrance of $E1$ transitions is taken into account by dividing the F_W by 10^4 before calculating f_ν.

In order to discuss the implications of these lifetime limits of the intrinsic states, it is useful to consider the ''hindrance per degree of K forbiddenness'' or reduced hindrance factors for the decays. The reduced hindrance factor is defined as

$$f_\nu = \{T^\gamma_{1/2}/T^W_{1/2}\}^{1/\nu}, \tag{7}$$

where $T^\gamma_{1/2}$ is the partial γ-ray half life, $T^W_{1/2}$ is the Weisskopf single-particle half-life estimate, and ν is the degree of K forbiddenness, $\Delta K - \lambda$. In order to take account of the generally observed strong $E1$ hindrance compared with the Weisskopf estimates [18,19] and, therefore, to allow comparisons with the strength of other multipolarities, the $E1$ $T^W_{1/2}$ value is multiplied by 10^4 before f_ν is calculated. The reduced hindrance limits for the transitions which decay from the $K^\pi = 28^-$, $K^\pi = (29^+)$, $K^\pi = 30^+$, and $K^\pi = (34^+)$ intrinsic states are shown in Table VII. Upper limits of $f_\nu \leqslant 20$ are determined. This may be compared with $f_\nu = 25$ for the $E1$ decay of the $K^\pi = 25^+$, 220 ns isomer [10].

In Ref. [10] the decay of the high-K states in ^{178}W was discussed on the basis of the f_ν reduced hindrance values for the transitions. It was reasoned that large f_ν values (> 20) signified that the γ-ray intensity decay path would follow the K selection rule and transitions would decay via the route with the minimum change in K. Under these circumstances, K was reasoned to be a good quantum number even at these high seniorities. However, when the f_ν values were small (< 2), then the decay path would proceed by the route with the highest transition energy as was observed in, for example, ^{176}W [20]. In the intermediate region, $2 < f_\nu < 20$, most of the decays proceed via the minimum changes in K, but there are some competing branches, as was observed in, for example, ^{174}Hf [21]. The new decays in ^{178}W from the

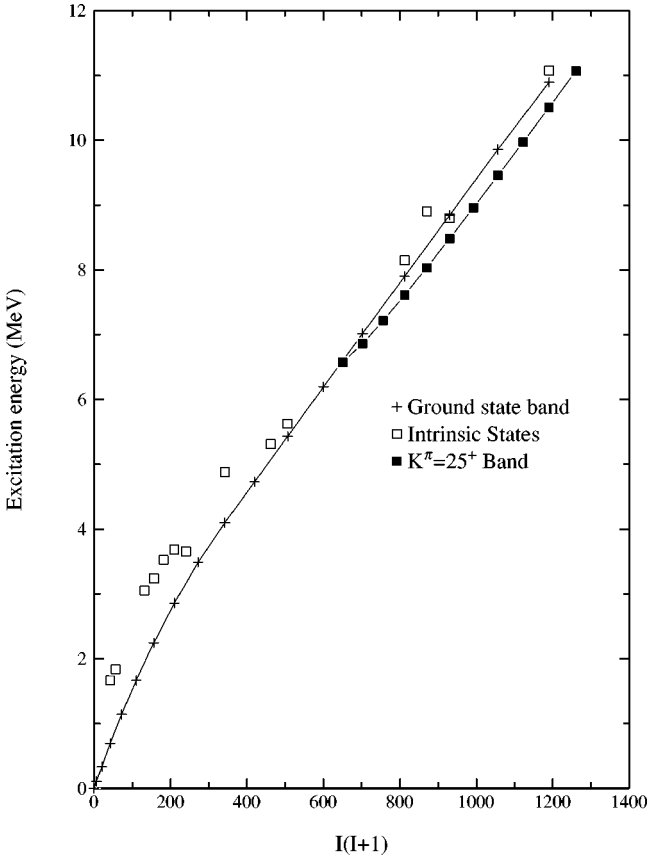

FIG. 4. Excitation energy plotted against $I(I+1)$ for the ground-state band (crosses) and intrinsic states (squares) in ^{178}W. The full $K^{\pi}=25^{+}$ band (filled squares) is yrast over the entire angular momentum range.

$K^{\pi}=28^{-}$, $K^{\pi}=(29^{+})$, $K^{\pi}=30^{+}$, and $K^{\pi}=(34^{+})$ intrinsic states all have upper limit f_{ν} values <20 (see Table VII). These decays may indeed be reasonably well retarded and the K quantum number may remain a good quantum number, even up to states with a seniority of ten, however, improved half-life data are required in order to provide a critical evaluation. Figure 4 shows that these $K^{\pi}=28^{-}$, $K^{\pi}=(29^{+})$, $K^{\pi}=30^{+}$, and $K^{\pi}=(34^{+})$ intrinsic states are all near yrast.

D. Total aligned angular momentum, I_x, and pairing correlations

The $K^{\pi}=30^{+}$ state is the highest-K state, observed to date, with more than one rotational transition which, therefore, allows its dynamic moment of inertia to be extracted. It might be intuitively expected that static pairing should be greatly reduced for this band because there are four unpaired protons and four unpaired neutrons. If pairing is greatly reduced then the kinematic and dynamic moments of inertia, $\mathfrak{I}^{(1)}$ and $\mathfrak{I}^{(2)}$, should be equal. It has previously been observed [9] that this is not the case for the eight-quasiparticle $K^{\pi}=25^{+}$ band in ^{178}W, where $\mathfrak{I}^{(1)}>\mathfrak{I}^{(2)}$ and this observation is contrary to the idea of simple classical rigid body rotation with no contribution from single-particle alignments [6,22].

In order to discuss these moments of inertia it is useful to use the same representation employed by Purry *et al.* [9,10] and Shimizu *et al.* [6] for the total aligned angular momentum, I_x, versus rotational frequency, ω. The values, I_x, for the $K^{\pi}=15^{+}$, $K^{\pi}=25^{+}$, $K^{\pi}=28^{-}$, $K^{\pi}=30^{+}$, and the ground-state-band, $K^{\pi}=0^{+}$, in ^{178}W are shown in Fig. 5. The ''apparent alignment'' in this figure is obtained from the extrapolation of the rotational axis component of the angular momentum, I_x, to zero rotational frequency. For the $K^{\pi}=25^{+}$ band it was previously noted [9] that the value at the intercept, measured in the present data to be $2.6\pm0.1\hbar$, was consistent with the Coriolis effect on the aligned angular momentum of the $h_{9/2}$ $1/2^{-}[541]$ proton in its eight-quasiparticle configuration. Calculations in Ref. [7] show that the Coriolis effect and, therefore, the net alignment, for the $h_{9/2}$ nucleon persists, despite reduced pairing. This is because the proton Fermi level is close to the $\Omega=1/2^{-}$ orbital, whereas, the $i_{13/2}$ neutron alignment drops because the neutron Fermi level is higher in the shell, between the $\Omega=7/2^{+}$ and $\Omega=9/2^{+}$ orbitals. In a similar manner the total aligned angular momentum, I_x, at zero rotational frequency for the $K^{\pi}=28^{-}$ band is $2.7\pm0.1\hbar$ because its configuration also contains the $h_{9/2}$ $1/2^{-}[541]$ proton. In contrast, the new $K^{\pi}=30^{+}$ band shows a value of approximately zero ($0.0\pm0.1\hbar$), which is consistent with it having no alignable high-j, low-Ω particles in its eight quasiparticle configuration. Indeed compared with the $K^{\pi}=25^{+}$ configuration, the configuration for this band has the $1/2^{-}[541]$ proton replaced by the $11/2^{-}[505]$ proton.

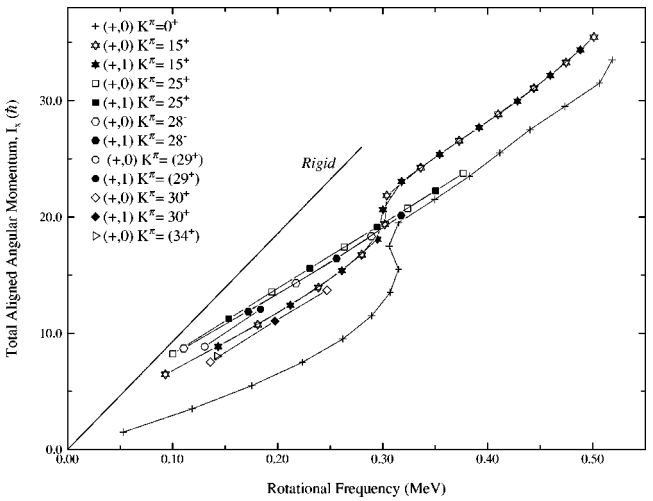

FIG. 5. Total aligned angular momentum for $K^{\pi}=25^{+}$, $K^{\pi}=28^{-}$, and $K^{\pi}=30^{+}$, and the ground-state band $K^{\pi}=0^{+}$ in ^{178}W as a function of rotational frequency. The solid line represents a rigid rotor with a moment of inertia of $85\hbar^{2}$ MeV^{-1}.

From Fig. 5, the kinematic and dynamic moments of inertia can easily be deduced by $\mathfrak{I}^{(1)}=\hbar I_x/\omega$ and $\mathfrak{I}^{(2)}=\hbar dI_x/d\omega$. These moments of inertia are shown for the $K^{\pi}=25^{+}$, $K^{\pi}=28^{-}$, $K^{\pi}=(29^{+})$, $K^{\pi}=30^{+}$, and $K^{\pi}=(34^{+})$ bands in Table VIII. It can be observed that the dynamic moment of inertia for the $K^{\pi}=25^{+}$ band, $\mathfrak{I}^{(2)}=51\hbar^{2}$ MeV^{-1}, is very much greater than that of the ground-state band of $29\hbar^{2}$ MeV^{-1}. However, this still only represents 60% of the rigid-body value of $85\hbar^{2}$ MeV^{-1} shown by the full line in Fig. 5. The $K^{\pi}=25^{+}$ band, appears in some sense, to form a ''barrier'' in total aligned angular

TABLE VIII. Kinematic $\mathfrak{I}^{(1)}$ and dynamic $\mathfrak{I}^{(2)}$ moments of inertia for the $K^\pi = 25^+$, 28^-, (29^+), 30^+, and (34^+) band in ^{178}W.

K^π	Bandhead $\mathfrak{I}^{(1)}$ $\hbar^2$/MeV	Gradient $\mathfrak{I}^{(2)}$ $\hbar^2$/MeV
25^+	82.2	51.0
28^-	78.8	53.8
(29^+)	67.8	60.5
30^+	55.8	55.9
(34^+)	56.4	[a]

[a]Insufficient points for calculation of $\mathfrak{I}^{(2)}$ for the $K^\pi = (34^+)$ band, since only one excited state is known in the band.

momentum beyond which no bands cross at low rotational frequency [7]. These observations may be reconciled with the fact that the ground-state band (below the first band crossing) has all particles fully paired and, therefore, the lowest moment of inertia. In contrast, the eight quasiparticle bands have eight unpaired particles, which are expected to lead to a substantial erosion of the nuclear pairing force and, therefore, a larger moment of inertia. One important feature of this figure and Table VIII is that the $K^\pi = 30^+$ band is the only band which has equality in its dynamic and static moments of inertia, $\mathfrak{I}^{(1)} = 55.8\hbar^2$ and $\mathfrak{I}^{(2)} = 55.9\hbar^2$ MeV^{-1}. This is precisely the behavior that would be expected for a rigid body. However, these values are still very much less than the $85\hbar^2$ MeV^{-1} rigid-body value. The $K^\pi = 30^+$ band, therefore, represents a better rotor than the $K^\pi = 25^+$ band, with no apparent alignment, but it still does not show a fully rigid moment of inertia even with eight unpaired particles. This is consistent [7] with the substantial pairing energy obtained in the Lipkin-Nogami calculations (see Sec. IV B) given in Table V, with $\Delta_n = 599$ keV and $\Delta_p = 707$ keV.

In Ref. [7] Dracoulis *et al.*, argued that if pairing correlations persist for these high-seniority states then, despite adding nucleons (not the $h_{9/2}$ proton), the apparent alignment decreases. The implication is that the fall in alignment, caused by the reduction of pairing, is greater than the effect of an underlying increase in the collective moment of inertia which, when using the reference appropriate to the low-seniority states, would lead to an apparent increase in alignment. For these new data in the present work the alignments of the 10 quasiparticle $K^\pi = (29^+)$ and $K^\pi = (34^+)$ bands can be compared with their respective underlying configurations, the $K^\pi = 30^+$ and $K^\pi = 25^+$ bands coupled to an additional two neutrons $(7/2^-[503] \otimes 1/2^-[521])$ in each case. This comparison is shown in Fig. 5. It can be seen that the alignment indeed reduces for the $K^\pi = (29^+)$ band compared with the $K^\pi = 25^+$ band, which seems to indicate that pairing correlations are still having an effect, at least at the eight-quasiparticle level. However, the alignment apparently does not reduce in the $K^\pi = (34^+)$ band (for which there is only a single data point) compared with the $K^\pi = 30^+$ band.

One interpretation of this is that the behavior of the $K^\pi = (34^+)$ band is just that expected if the pairing is indeed already quenched in the $K^\pi = 30^+$ band, as implied by the equality of its dynamic and static moments of inertia (and the corresponding absence of net alignment) discussed previously. The further implication is that those moments of inertia (close to $56\hbar^2$ MeV^{-1}) correspond to the *underlying unpaired moment of inertia* for ^{178}W. The blocking of two extra neutrons to form the $K^\pi = (34^+)$ configuration from the $K^\pi = 30^+$ configuration (see Table V) can then have no additional effect on the pairing and, therefore, on the apparent moment of inertia. The absence in the present results of rotational transitions above the first member of the $K^\pi = (34^+)$ band means, unfortunately, that the dynamic moment of inertia is not defined. A crucial test of this proposition would be provided by such higher data points which, if the proposition is valid, should define the same slope for the $K^\pi = (34^+)$ and $K^\pi = 30^+$ bands in the I_x versus $\hbar\omega$ curves of Fig. 5.

As stated previously, shell effects have been identified [8] as a mechanism which would produce moments of inertia different from the classical rigid-body values, even when pairing is quenched. Furthermore, zero-pairing tilted-axis-cranking calculations, of the type described by Frauendorf [23] have been carried out [24] for the $K^\pi = 30^+$ band in ^{178}W. These calculations are successful in reproducing $\mathfrak{I}^{(1)} = \mathfrak{I}^{(2)} = 56\hbar^2$ MeV^{-1}, and lend support to the interpretation proposed here.

V. SUMMARY

In summary, three new high-K multiquasiparticle intrinsic states, $K^\pi = (29^+)$, $K^\pi = 30^+$, and $K^\pi = (34^+)$, based on ten, eight, and ten, unpaired nucleons, respectively, have been assigned in ^{178}W. Configuration-constrained potential energy surface calculations indicate that the nucleus retains stably deformed axially symmetric shapes. This evidence, coupled with the experimental γ-ray decay rates, suggests that K remains a good quantum number in these highest-seniority intrinsic state configurations. The aligned angular momenta of the $K^\pi = (29^+)$, $K^\pi = 30^+$, and $K^\pi = (34^+)$ bands are observed to be lower than those of the other eight quasiparticle, $K^\pi = 25^+$ and $K^\pi = 28^-$ bands in ^{178}W. These properties have been interpreted as evidence for the quenching of pairing and imply a saturation of the low-frequency, high-seniority moments of inertia for ^{178}W at a value of $56\hbar^2$ MeV^{-1}.

ACKNOWLEDGMENTS

The authors would like to thank D.C. Radford for the use of the ''RADWARE'' software [13], W.T. Milner [14] for the use of the ''UPAK'' software, and H.-Q. Jin for the use of ''JINWARE.'' D.M.C., S.L.K., and C.W. acknowledge financial support from the EPSRC and A.T.R. acknowledges support from the University of Liverpool during the course of this work. S. Frauendorf is thanked for communicating the results of the tilted-axis-cranking calculations prior to publication.

[1] A. Bohr, B.R. Mottelson, and D. Pines, Phys. Rev. **111**, 936 (1958).
[2] S.T. Belyaev, Mat. Fys. Medd. K. Dan. Vidensk. Selsk. **31**, 11 (1959).
[3] S.T. Belyaev, Nucl. Phys. **24**, 322 (1961).
[4] A.B. Migdal, Nucl. Phys. **13**, 655 (1959).
[5] J. Bardeen, L.N. Cooper, and J.R. Schrieffer, Phys. Rev. **108**, 1175 (1957); N.N. Bogolyubov, Zh. Éksp. Teor. Fiz. **34**, 58 (1958) [Sov. Phys. JETP **34**, 41 (1958)].
[6] Y. Shimizu *et al.*, Rev. Mod. Phys. **61**, 131 (1989).
[7] G.D. Dracoulis, F.G. Kondev, and P.M. Walker, Phys. Lett. B **419**, 7 (1998).
[8] V.V. Pashkevich and S. Frauendorf, Sov. J. Nucl. Phys. **20**, 588 (1975).
[9] C.S. Purry, P.M. Walker, G.D. Dracoulis, T. Kibédi, S. Bayer, A.M. Bruce, A.P. Byrne, M. Dasgupta, W. Gelletly, F.G. Kondev, P.H. Regan, and C. Thwaites, Phys. Rev. Lett. **75**, 406 (1995).
[10] C.S. Purry, P.M. Walker, G.D. Dracoulis, T. Kibëdi, F.G. Kondev, S. Bayer, A.M. Bruce, A.P. Byrne, W. Gelletly, P.H. Regan, C. Thwaites, O. Burglin, and N. Rowley, Nucl. Phys. **A632**, 229 (1998).
[11] K. Jain, O. Burglin, G.D. Dracoulis, B. Fabricius, N. Rowley, and P.M. Walker, Nucl. Phys. **A591**, 61 (1995).
[12] I.Y. Lee, Nucl. Phys. **A520**, 641c (1990).
[13] D.C. Radford, Nucl. Instrum. Methods Phys. Res. A **361**, 297 (1995).
[14] W.T. Milner (private communication).
[15] K.S. Krane, R.M. Steffen, and R.M. Wheeler, Nucl. Data Tables **11**, 351 (1973).
[16] F. Dönau and S. Frauendorf, *Proceedings of the Conference on High Angular Momentum Properties of Nuclei, Oak Ridge, Tennessee, 1982*, edited by N.R. Johnson (Harwood Academic, New York, 1983); F. Dönau, Nucl. Phys. **A471**, 469 (1987).
[17] F.R. Xu, P.M. Walker, J.A. Sheikh, and R. Wyss, Phys. Lett. B **435**, 257 (1998).
[18] N.L. Gjørup, M.A. Bentley, B. Fabricius, A. Holm, J.F. Sharpey-Schafer, G. Sletten, and P.M. Walker, Z. Phys. A **337**, 353 (1990).
[19] T. Venkova, T. Morek, G.V. Marti, H. Schnare, A. Krämer-Flecken, W. Gast, A. Georgiev, G. Hebbinghaus, R.M. Lieder, G. Sletten, K.M. Spohr, K.H. Maier, and W. Urban, Z. Phys. A **A334**, 417 (1993).
[20] B. Crowell *et al.*, Phys. Rev. C **53**, 1173 (1996).
[21] N.L. Gjørup, P.M. Walker, G. Sletten, M.A. Bentley, B. Fabricius, and J.F. Sharpey-Schafer, Nucl. Phys. **A582**, 369 (1995).
[22] A. Bohr and B.R. Mottelson, Phys. Scr. **24**, 71 (1981).
[23] S. Frauendorf, in *Proceedings of the Workshop on Gammasphere Physics, Berkeley, California, 1995*, edited by M.A. Deleplanque, I.Y. Lee, and A.O. Macchiavelli (World Scientific, Singapore, 1996), p. 272.
[24] S. Frauendorf (private communication).